JOURNAL OF MATERIALS SCIENCE 23 (1988) 4132–4140

Ductilization and embrittlement during the crystallization of Ni–Ti–B glasses

N. MERK, D. G. MORRIS, M. A. MORRIS
Institute of Structural Metallurgy, University of Neuchâtel, 2000 Neuchâtel, Switzerland

The fracture responses of three Ni–Ti–B glasses have been studied during the very early stages of crystallization. Comparison of alloys leads to a separation of relaxation and crystallization effects. The tendency toward reductilization in the presence of a small quantity of crystalline particles is directly related to the fine distribution and very small size of these particles which tends to interrupt concentrated shear without causing significant localized failure. Such particles thereby tend to distribute the plastic deformation homogeneously and to compensate the simultaneous relaxation embrittlement.

1. Introduction

Relaxation and crystallization embrittlement have previously been reported for a wide range of transition metal–metalloid glasses [1, 2]. The relaxation phenomenon has been attributed to the loss of free volume leading to the difficulty of plastic deformation. The embrittlement intensity and flow behaviour depend on the atomic and electronic nature of the elements [3, 4]. A tendency to phase separation or clustering during relaxation has also been evoked as a cause of embrittlement [5]. In $Fe_{40}Ni_{40}B_{20}$ glass, the formation of an extremely fine dispersion of $(Fe, Ni)_3B$ particles has been found to embrittle the glass when their size exceeds 2.5–3 nm [6]. Auger analysis of $Fe_{40}Ni_{40}P_{14}B_6$ [7] indicates that during annealing segregation occurs into discrete regions of less than 6 nm in size. These regions of high phosphorus (P) concentration cause embrittlement and are nuclei for crystals less ductile than the matrix. Thus subsequent crystallization embrittlement would be expected.

Such a loss of ductility is normally catastrophic and can prevent practical applications of metallic glasses. It would be desirable to obtain alloys for which the ductility remains high even after introducing crystalline phases (formed during crystallization or due to a low cooling rate). In very rare cases, a partial reductilization of the material at the onset of crystallization has been reported, for example $Fe_{41}Ni_{41}B_{18}$ is reductilized when primary crystals of γ(Fe, Ni) appear [8]. If ageing continues, a brittle Fe_3B phase appears which leads to the reappearance of embrittlement. The partial ductilization of Fe–B alloys during crystallization has been attributed to the presence of a few small, soft particles [9]. The creation of these soft particles within the glass liberates new free volume and hence the glass reacquires a facility for plastic deformation. The subsequent embrittlement which occurs when ageing continues has been explained by the enrichment of the matrix in boron which tends to trap the free volume and hence to embrittle the material. Depending on their composition, Fe–Ni–Zr alloys containing niobium or tantalum [10] tend to be more or less ductile even for a significant fraction of crystallization and in the presence of hard particles. $Fe_{40}Ni_{20}Zr_9Nb$ has the best ductility during crystallization of all the alloys studied, remaining ductile up to 30% crystallization, and in particular has the smallest average crystal size (compared to the other alloys). This observation suggests a certain relationship between the size of the particle present and the overall ductility of the material.

This paper describes the changes in fracture behaviour observed during the crystallization of a series of Ni–Ti–B glasses. These glasses form different phases during crystallization and thus it is possible to relate the mechanical response to the phase nature as well as to the distribution of these crystalline particles. In this paper we analyse the reductilization effect of small amounts of crystallinity, and in a second paper we develop a model for the crystallization embrittlement which follows.

2. Experimental details

Three alloys of composition: $Ni–B_{19.1}Ti_{2.1}$ (alloy A), $Ni–B_{18.2}Ti_{3.8}$ (alloy B) and $Ni–B_{17.9}Ti_3$(alloy C) have been melt spun (courtesy of Professor Güntherodt, University of Basel) as ribbons $\sim$9 mm wide and $\sim 20\,\mu m$ thick. Microstructural studies were carried out using a variety of annealing conditions in parallel with toughness tests and fracture surface examinations. Heat treatments were performed in a salt bath or in a furnace under argon atmosphere. The microstructures were characterized (crystal nature, size and distribution) using a Hitachi H-700 TEM operating at 200 kV. Fracture toughness tests were performed in an Instron testing machine on polished specimens with a 2 mm long centre notch introduced by spark erosion (before heat treatment) using a 100 μm thick copper-foil electrode. The 2.5 cm long samples were glued to plate grips and pulled at a constant displacement rate of 0.2 mm min^{-1}. The localized deformation at the notch was independent of sample irregularities (or

0022–2461/88 $03.00 + .12

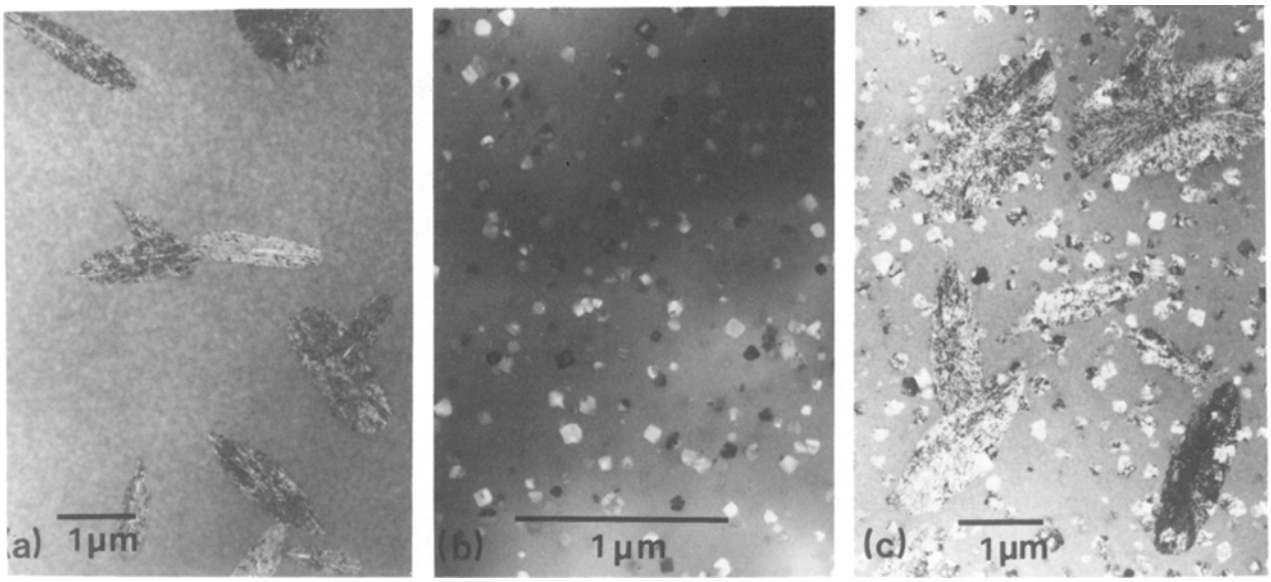

Figure 1 Typical microstructure of partially crystallized alloys: (a) alloy A after 24 h at 280° C; (b) alloy B after 8 h at 300° C and (c) alloy C after 8 h at 300° C.

grip stress concentrations) leading to highly reproducible (± 15 %) data. For each condition four to six samples were tested, obviously imperfect samples were discounted, and finally the fracture toughness estimated to within ± 5 to 10 %. Fracture toughness was calculated from the failure load using standard stress-intensity formulae. The resulting fracture surfaces have been observed and characterized using a Cambridge 250 Scanning Electron Microscope.

3. Results

A typical microstructure of each partially crystallized alloy is shown in Fig. 1. Alloy A (Fig. 1a) crystallizes following a eutectic process leading to the formation of a mixture of orthorhombic Ni_3B and fcc nickel. Alloy B (Fig. 1b) contains primary crystals of τ phase ($M_{23}B_6$). Alloy C (Fig. 1c) crystallizes by the simultaneous formation of three phases – the lamellar, cigar-shaped eutectic colonies (as in alloy A) together with the small faceted τ phase crystals (as in alloy B) and small irregular-shaped crystals of fcc nickel. Details of the crystallization kinetics have been reported previously [11].

The results of the toughness tests following heat treatment at 300° C are presented in Fig. 2. For each alloy a similar evolution of the fracture toughness has been obtained as crystallization takes place at different annealing temperatures. At the fully crystalline state all three alloys have lost as much as $\frac{3}{4}$ of the original toughness. The evolution of toughness for each alloy is not identical, however. While alloy A (Fig. 2a) undergoes a sharp and continuous decrease in toughness, alloy C (Fig. 2c) shows a small initial increase in toughness (this increase is much more prominant at the highest annealing temperature (350° C, see also Fig. 7) and not observed at the lowest temperature) and alloy B (Fig. 2b) shows essentially two stages of embrittlement with a short toughness plateau between the two stages. The toughness value at the plateau for alloy B increases with temperature, 25 $MN\,m^{-3/2}$ at 300° C, 27 $MN\,m^{-3/2}$ at 350° C and 34 $MN\,m^{-3/2}$ at 375° C. As shown in Fig. 2b, annealing for only 15 min leads already to a toughness reduction of 2 $MN\,m^{-3/2}$. Since the fraction of crystalline material does not exceed 10^{-6} during the first hour of heat treatment, the observed embrittlement can be attributed totally to the relaxation effect.

For alloy B, annealing from 2 to 6 h leads to an increase in the fraction of crystalline material from 10^{-5} to 7×10^{-3}. During this period the average crystal size (10 nm at 2 h) increases to 30 nm. Two possible explanations can be proposed to explain the fracture behaviour during this early crystallization stage of the alloy. One explanation is that the relaxation embrittlement reaches an end before crystallization embrittlement starts and the other possibility is that the continuing relaxation embrittlement is temporarily balanced by a ductilization tendency due to the presence of the very first crystals, with crystallization embrittlement taking place subsequently. As will be shown later, this second possibility seems more likely.

In our alloys, both in the glassy state as well as the partially crystalline state, fracture occurs by a shear mechanism on a well defined macroscopic shear plane oriented at 45° to the tensile axis. Initially, the fracture surfaces of all three alloys contain the two typical zones of fractured glassy metals: the shear offset which is a smooth zone formed during initial shearing and the veined zone formed during final fracture. In order to demonstrate the morphology change during crystallization, a sequence of fracture surfaces of alloy A and B is presented in Fig. 3. As crystallization takes place, several changes occur. In particular it may be noted that the vein pattern has changed into a dimple structure, reflecting the influence of the internal microstructures (Figs 1a and b).

Nevertheless in both cases as more and more crystallization occurs, the offset decreases and the density of dimples increases. In this sense, the offset (Δ) and the average dimple size (D) can be chosen as parameters characterizing the fracture surfaces and the

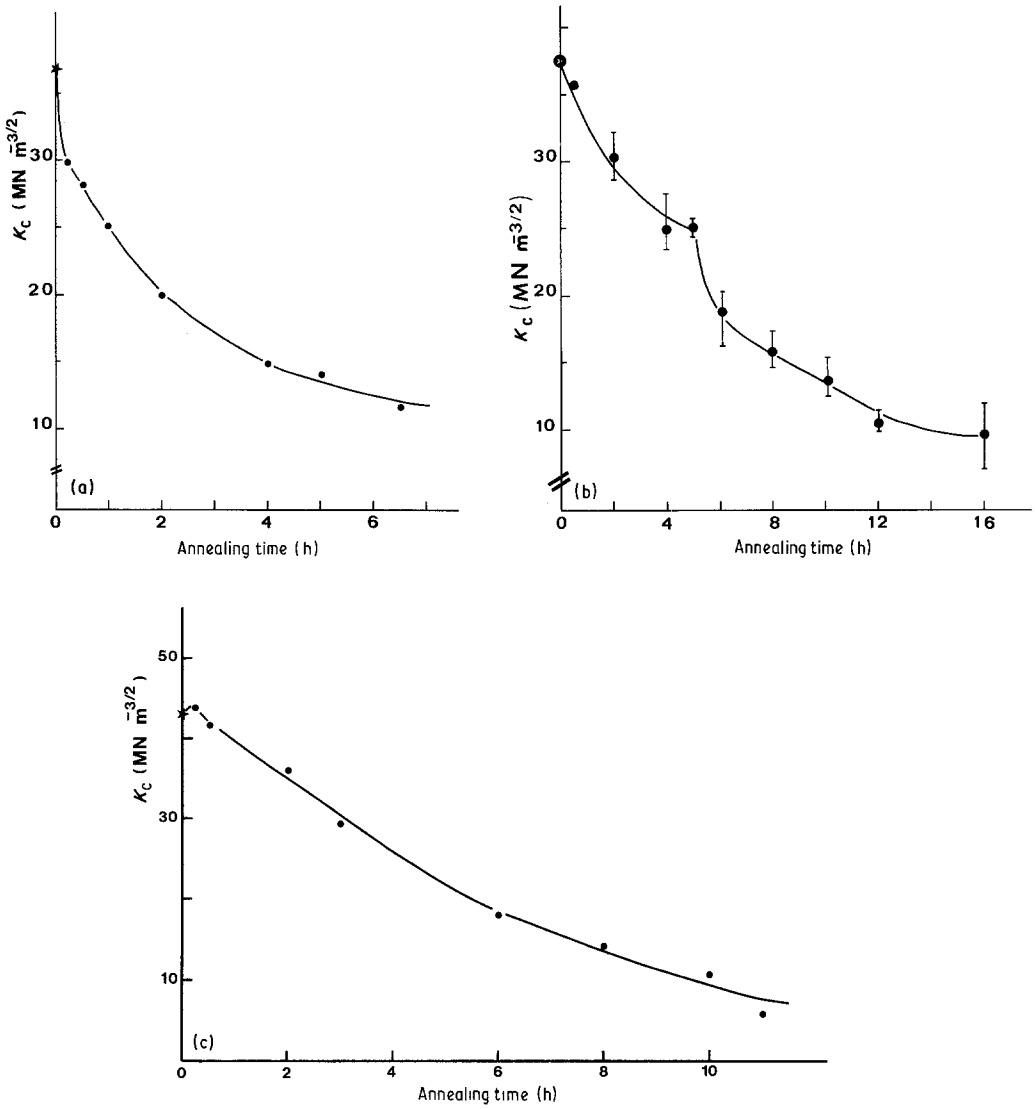

Figure 2 Toughness evolution during heat treatment at 300° C for (a) alloy A; (b) alloy B and (c) alloy C.

changes occurring. The decreases in offset and dimple size during annealing of alloys A and B at three different temperatures are presented in Fig. 4. For alloy A, the offset and the dimple size decrease at very much the same rates for a given temperature and, furthermore, there is a clear correspondence between D and Δ for each fracture surface condition (see Fig. 3I). In comparison, for alloy B, the dimple size decreases at a much faster rate than the offset (see Fig. 3II). For alloy C, the fracture surface parameters (Δ and D) decrease during crystallization in much the same way as alloy B.

The importance of the fracture surface morphology in relation to the toughness is indicated by Fig. 5 where a clear relationship between the toughness and the square root of the offset is seen for all three alloys. The values of the slopes of the lines obtained are 16 GN m^{-2} for alloy A, 10–22 GN m^{-2} for alloy B and 20 m^{-2} for alloy C.

4. Discussion

Independent of the alloy composition, a loss of ductility seems unavoidable during annealing. Both relaxation and crystallization have an embrittlement effect on glasses. Nevertheless, as illustrated in Fig. 2c, at the very early stages of crystallization a slight ductilization may be achieved in some cases. For example, during the first hour at 300° C, the alloy C shows a slight increase in ductility. During this period, the fracture of crystalline material reaches 10^{-4} with an average size of the small particles (τ and f c c nickel) of 35 nm (after 1 h) and an average size of eutectic colonies of 250 nm (after 1 h).

Since alloy B shows only relaxation embrittlement during the first hours of heat treatment (at 300° C) a comparison of alloys B and C will allow a separation of the different effects. In order to make this separation we shall assume that the relaxation effect and the kinetics of relaxation are similar for the two alloys. Considering the very slight difference in composition between the alloys and the fact that the ribbons have been made at essentially the same cooling rate, under the same casting conditions, the glass transition temperature T_g of the alloys should be very close to each other. This assumption has been confirmed in several previous studies in which a small change in composition has been shown to lead to only a small change in T_g [12–14]. In addition, it has been reported on several occasions that the relaxation kinetics in a given transition metal–metalloid system are similar for alloys containing between 16.5 to 28.9 at % of metalloid [15, 16] (around an eutectic composition).

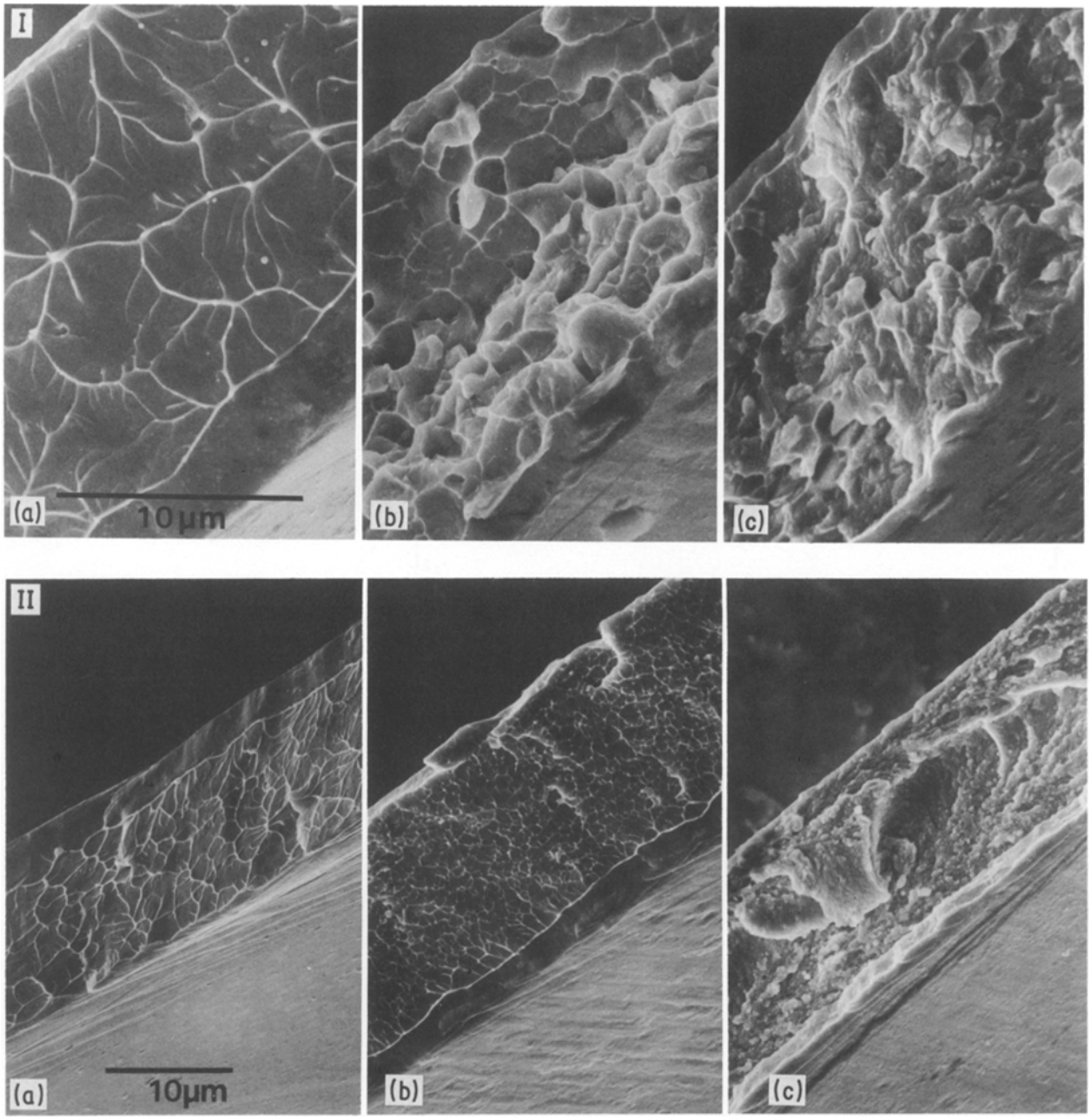

Figure 3 Fracture surface evolution during crystallization of (I) alloy A after 2, 5 and 7 min at 350° C and (II) alloy B after 4, 10 and 17 min at 350° C.

Thus, with the assumption of the same relaxation kinetics during annealing (for each temperature) for the two alloys B and C, the superposition of the fracture toughnesses allows the various factors affecting toughness to be separated. Figs 6 and 7 show the superposition of the two toughness curves (alloys Band C) at 300° C and 350° C. In the period of 0 to 1 h, at 300° C, alloy B undergoes relaxation embrittlement only while during this period alloy C already contains crystals of a certain size which compensate the matrix relaxation embrittlement. Thus the difference between the toughnesses of the two alloys (reported in Figs 6c and 7c) from the initial value up to the first intersection of the two curves determines the region of crystallization ductilization of alloy C. Since the initial toughness values are not equal, an upper and lower limit of the ductilization domain can be defined by direct superposition of the experimental toughness data (Figs 6a and 7a) or by displacing the toughness data to an identical initial value for the two glasses (Figs 6b and 7b).

The same analysis performed on the 350° C data (Fig. 7) provides another example of this behaviour. In the period of 0 to 6 min, corresponding to the relaxation embrittlement of alloy B, the fraction of crystalline material in alloy C reaches 2×10^{-2}. After 6 min, the eutectic and small crystals are respectively of size 600 nm and 60 nm. It is over this period that ductilization of alloy C is observed.

In a similar fashion, for the period of time during which alloy B shows a tendency toward ductilization, the difference in toughness of alloys B and C determines the ductilization domain of this alloy. An examination of the microstructures of alloy B over

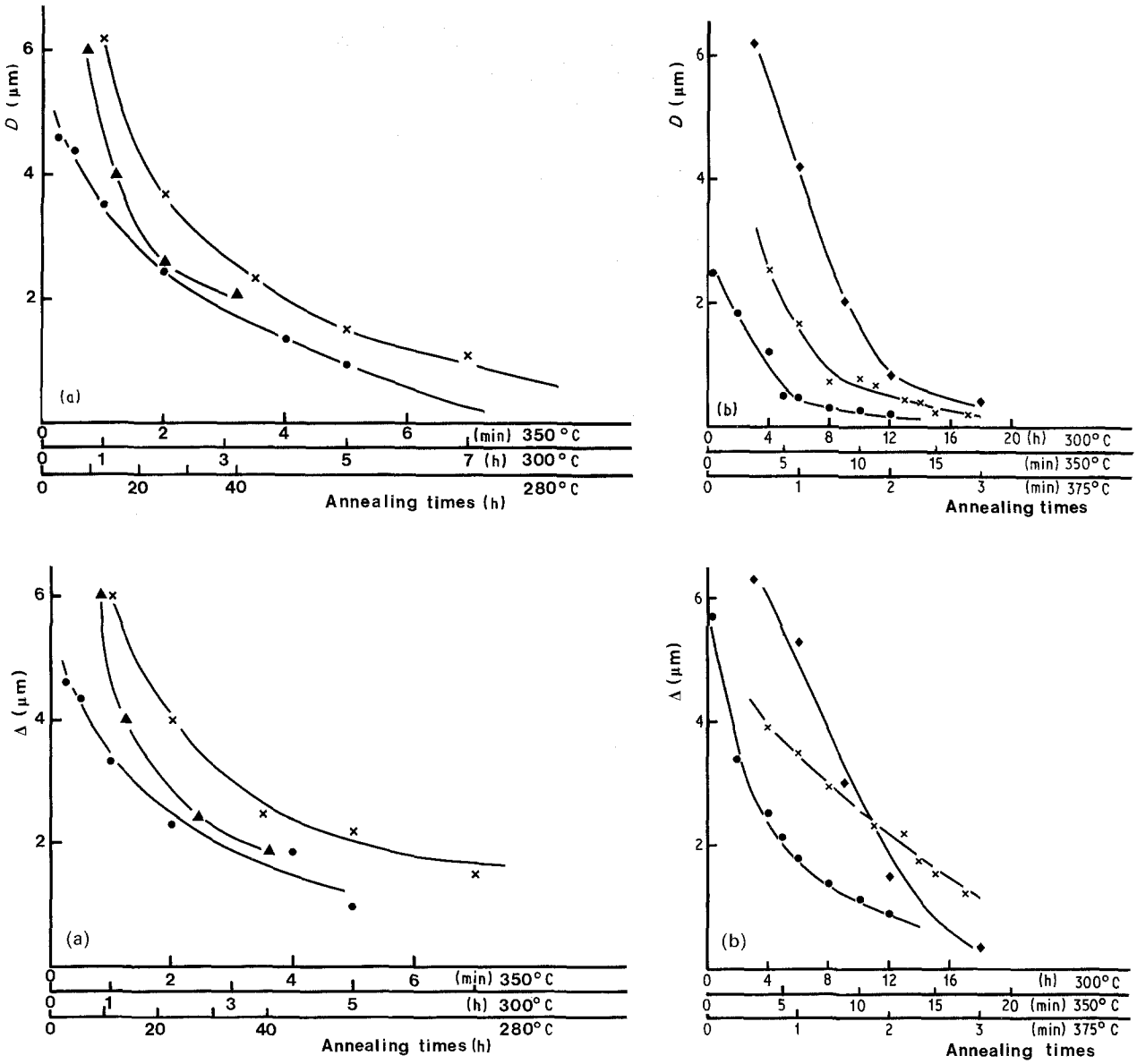

Figure 4 Variation of dimple size and offset with annealing time at three different annealing temperatures (× 350° C, ● 300° C, ▲ 280° C, ◆ 375° C) for (a) alloy A and (b) alloy B.

these stages confirms that the reductilization tendency coincides with the first appearance of crystalline particles.

In Table I the microstructural parameters corresponding to the condition of maximum ductilization are summarized. The only common parameter between all conditions of ductilization is the size of the small crystalline particles, namely about 25–35 nm, while the amount of crystallinity may vary from about 10^{-5} to near 10^{-2}: the eutectic particles do not appear to play a dominant role in determining the ductilization effect.

In comparison with other glassy alloys in which crystallization ductilization has been observed, it seems reasonable to associate ductilization with a very small size of the crystalline particles. For example partially crystallized Fe–Ni–Zr alloys are ductile [10] before the average crystal size reaches 50 nm, independent of the crystal density. The crystals formed in this particular case, just as the present τ and orthorhombic

TABLE I Microstructural conditions corresponding to the maximum extent of ductilization of alloys B and C

		Annealing temperature (° C)			
		260	300	350	375
Alloy C	Fraction crystalline	$< 10^{-4}$	10^{-5}	10^{-4}	–
	Size of eutectics	< 100 nm	120 nm	150 nm	–
	Size of τ/γ crystals	< 40 nm	25 nm	30 nm	–
	Distance between Eutectics	> 2 μm	6 μm	3 μm	–
	Distance between small crystals	> 0.8 μm	1.2 μm	0.6 μm	–
Alloy B	Fraction crystalline	–	10^{-3}	5×10^{-3}	$10^{-2,-3}$*
	Size of τ crystals	–	25 nm	30 nm	20–40 nm*
	Distance between crystals	–	0.5 μm	0.4 μm	0.3 μm*

*Values corresponding to the change in slope of toughness at the plateau observed during crystallization.

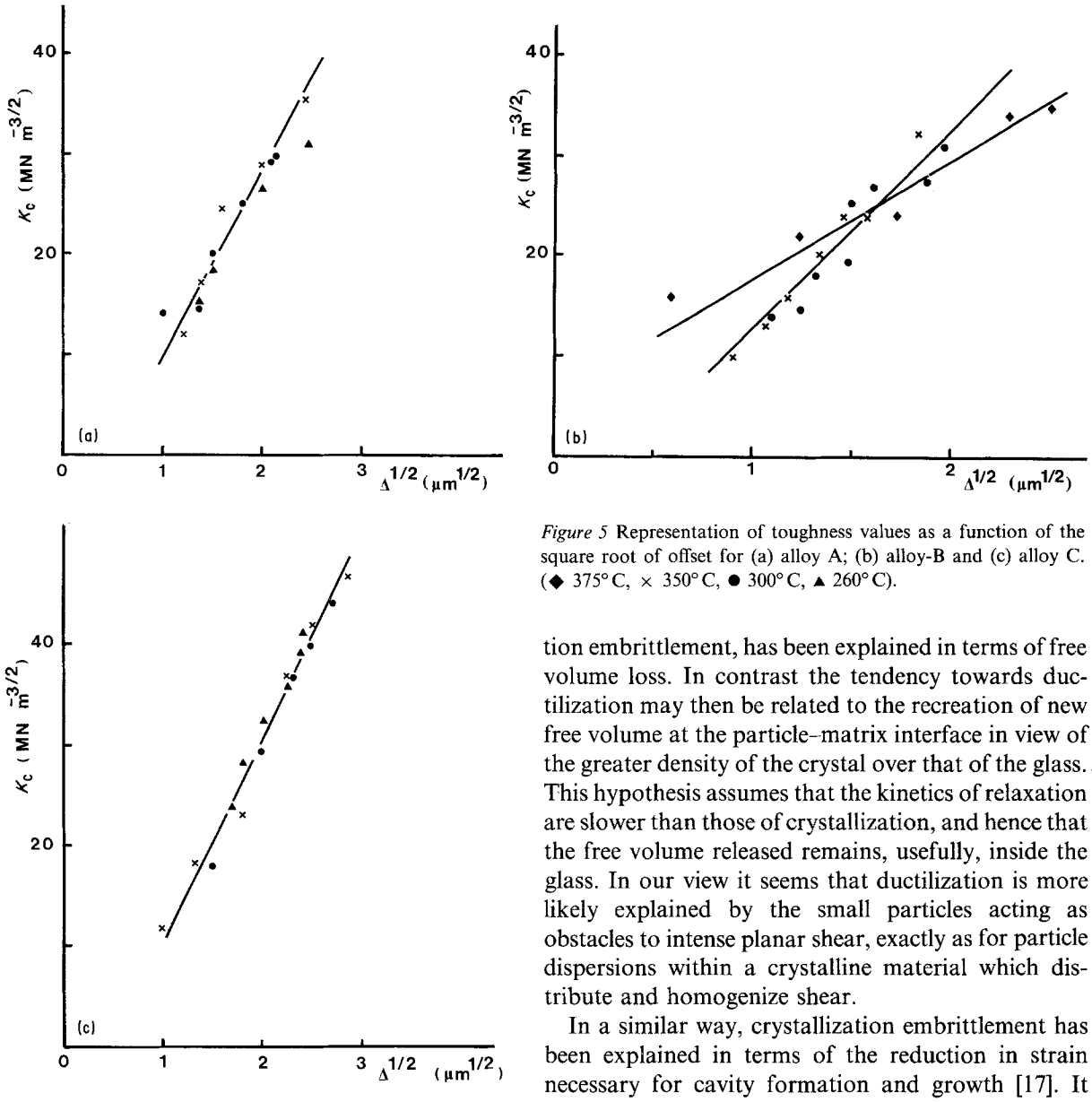

Figure 5 Representation of toughness values as a function of the square root of offset for (a) alloy A; (b) alloy-B and (c) alloy C. (◆ 375° C, × 350° C, ● 300° C, ▲ 260° C).

Ni_3B particles, can be considered as rather hard particles, in contrast to the soft particles studied by Hillenbrand *et al* [8, 9]. Rather it seems that crystal size instead of crystal nature, is the dominant factor determining ductilization. According to this, the observed ductilization in Fe–B glasses [8, 9] can be interpreted in terms of particle size rather than particle nature (hard or soft). For this alloy, the loss of ductility takes place when the Fe_3B particles have nucleated and the particle average size has then reached about 150 nm [9].

If the size criterion is taken as important for significant ductilization, the reason why a ductilization effect was not detected during crystallization of alloy A (and also for alloy C at 260° C) may be found. The first heat treatments used here produce already large particles corresponding to the end of the ductilization domain when crystallization embrittlement is already significant (bearing in mind that the crystallization process of alloy A is of eutectic type with a relatively fast crystal growth rate).

The ductilization effect is observed in association with two embrittlement effects. One of these, relaxation embrittlement, has been explained in terms of free volume loss. In contrast the tendency towards ductilization may then be related to the recreation of new free volume at the particle–matrix interface in view of the greater density of the crystal over that of the glass. This hypothesis assumes that the kinetics of relaxation are slower than those of crystallization, and hence that the free volume released remains, usefully, inside the glass. In our view it seems that ductilization is more likely explained by the small particles acting as obstacles to intense planar shear, exactly as for particle dispersions within a crystalline material which distribute and homogenize shear.

In a similar way, crystallization embrittlement has been explained in terms of the reduction in strain necessary for cavity formation and growth [17]. It follows that for crystallization ductilization to be observed stable cavities should not be easily formed at the particle–matrix interface. The dependence of particle size on stable cavity formation may be treated in terms of creating a critical stress concentration at the interface [18], and hence in terms of minimum necessary particle size. In addition, it may be that particles smaller than the shear band thickness (~ 20 nm [19]) may not yet be effective obstacles. Hence it is reasonable to suppose that for particles up to 25–30 nm in size (the condition of maximum ductilization shown in Table I) the probability of stable cavity formation is low. Thus, the addition of the two effects (slip band obstruction without yet the possibility of easy nucleation) determines the range of crystallization ductilization.

It is clear that growing particles, acting as stress raisers, will become stronger and stronger barriers against flow and hence more susceptible to cavity nucleation. The rate of cavity nucleation will increase with particle size and will eventually lead to the third domain of crystallization embrittlement.

Crystallization embrittlement is represented by the final fall in toughness (see Fig. 2) towards the values characteristic of the fully crystalline states. Fracture

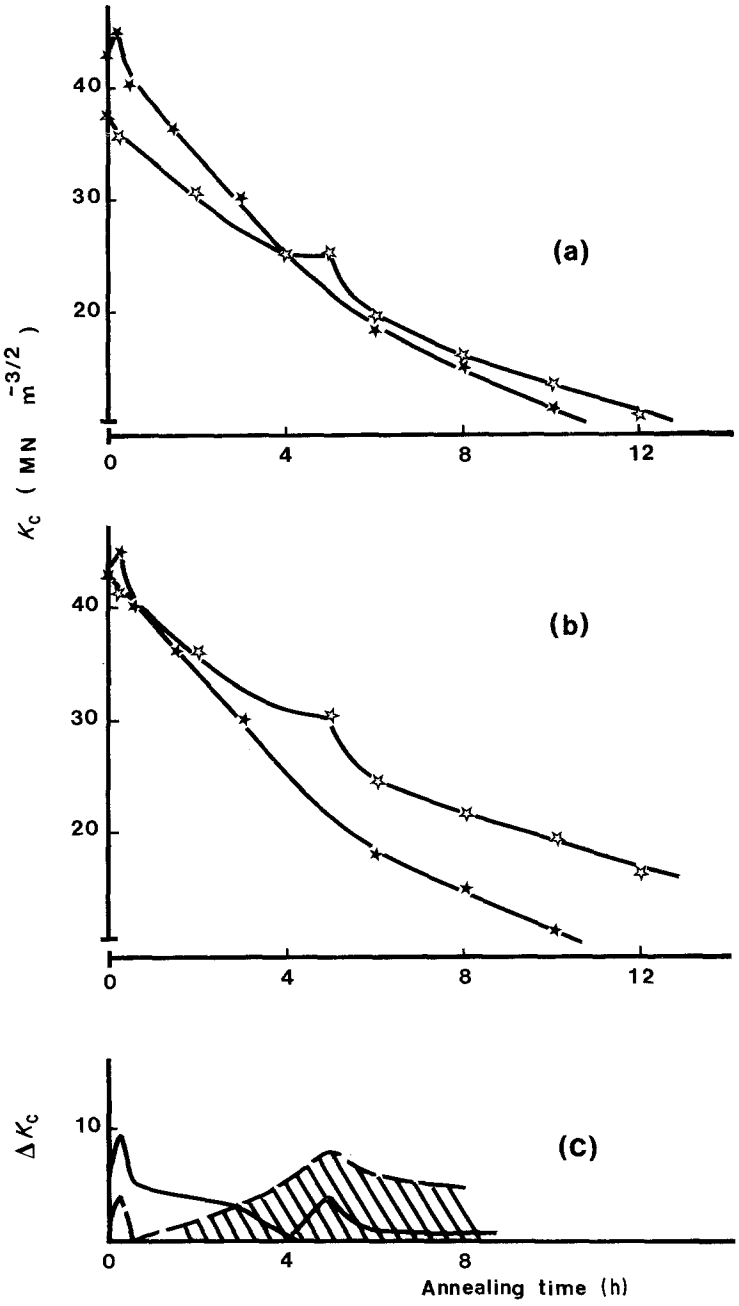

Figure 6 Superposition of toughness curves at 300° C for alloys B (☆) and C (★): (a) using the measured toughness values; (b) based on identical starting toughnesses for the two glasses; (c) the difference of toughness for the two alloys allowing the determination of the ductilization domain for each alloy. The two lines (continuous and dashed) indicate the range of ductilization according to the toughness values used for comparison (from (a) and (b) respectively). The shaded area shows the ductilization regime for alloy B and the open area that for alloy C.

occurs when the shear displacement reaches a critical value, the offset Δ measured on the fracture surfaces. The absence of work hardening in the glass (as well as in the partially crystallized glasses) allows us to relate the work done during shear fracture (G), the shear stress (τ_c) and the shear displacement (Δ). At failure

$$G_c = \tau_c \Delta \quad (1)$$

(assuming that all the work is introduced as plastic deformation without work hardening at the fracture surface). According to Irwin [20] the fracture toughness can be related to the strain energy release rate, as

$$K_{IC} = (EG)^{1/2}$$

by analogy, for the shear failure examined here, we can write

$$K_{IIIC} = (\mu G_c)^{1/2} \quad (2)$$

where μ is the shear modulus, thus

$$K_{IIIC} = (\mu\tau_c)^{1/2}\Delta^{1/2} \quad (3)$$

which corresponds to the relation observed in Fig. 5. Since the fracture toughness measured was based on the applied, longitudinal stress, the measured slope can best be related to about $(2\mu\tau_c)^{1/2}$. It is clear that this value is not a constant during crystallization (the shear modulus can increase by up to 30% during crystallization and also microhardness measurements performed on the present alloys show an increase of nearly 40% during crystallization). Nevertheless as can be seen in Fig. 5, the approximation of a constant slope is not unreasonable. Using literature values for the material parameters ($\mu = 50\,\mathrm{GN\,m^{-2}}$ and $\tau_c = \sigma_y/2 = 1.15\,\mathrm{GN\,m^{-2}}$ [21]) of nickel-based glasses, the slope $(2\mu\tau_c)^{1/2}$ is deduced to be $12\,\mathrm{GN\,m^{-2}}$ in reasonable agreement with the measured slopes from Fig. 5 (10–$20\,\mathrm{GN\,m^{-2}}$). Some of the difference between the experimental and the calculated slopes may arise in the work required for final fracture, namely the ductile parting of the regions between the cavities.

From the above discussion, and particularly in view of the virtual constancy of τ_c for a given alloy, it is

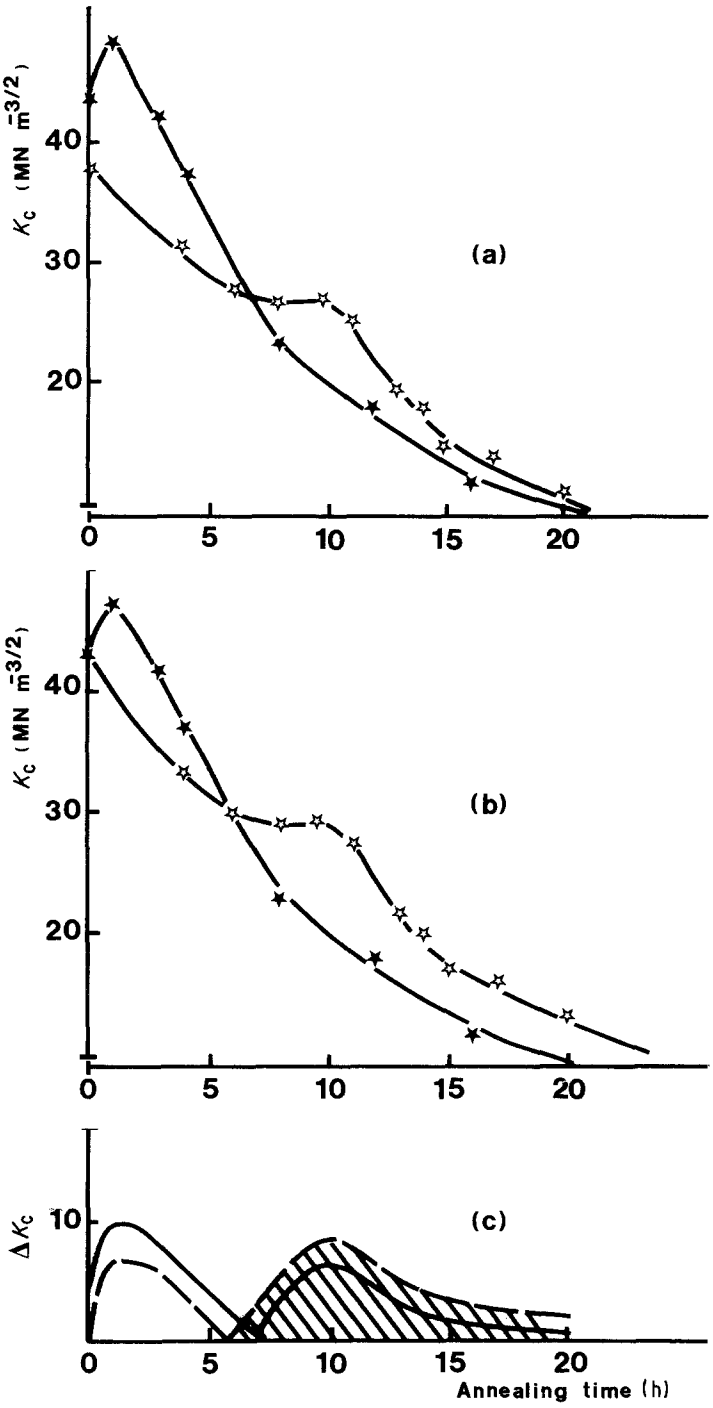

Figure 7 Superposition of toughness curves at 350° C for alloys B (☆) and C (★): details are the same as for Fig. 6.

clear that the critical shear displacement Δ takes on an especially significant meaning as a parameter characterizing failure. It has been shown that the values of Δ and D, the size of the dimples on the fracture surfaces, are closely related and also dependent on the types of particles present. This relationship, as well as an explicit model of the failure of semi-crystalline metallic alloys, will be treated in a later publication.

5. Conclusions

Different factors affecting the fracture behaviour during crystallization of three Ni–Ti–B glasses have been separated. A very first period of heat treatment corresponds to relaxation embrittlement and is followed and combined with a certain period of partial ductilization at the onset of crystallization. Such ductilization takes place when small particles (20–40 nm) are present which tend to inhibit the localized shear deformation characterizing the glass and thereby to homogenize shear. The ductilization effect is lost when the particles exceed a critical size for which cavitation at the particles becomes possible. The shear displacement necessary to cause such cavitation and then failure is representative of the toughness of the material.

References

1. F. E. LUBORSKY and J. L. WALTER, *J. Appl. Phys.* **47** (1976) 3638.
2. H. KIMURA and D. G. AST, Proceedings 4th International Conference on Rapidly Quenched Metals, Vol. 1 (edited by T. Masumoto and K. Suzuki) (Japan Institute of Metals) p. 457.
3. H. S. CHEN, J. T. KRAUSE and E. COLEMAN, *J. Non-Crystal. Solids* **8** (1975) 157.
4. *Idem., Scripta Metall.* **9** (1975) 787.
5. H. S. CHEN, *Mater. Sci. Engng* **26** (1976) 79.
6. J. PILLER and P. HAASEN, *Acta Metall.* **30** (1982) 1.

7. J. L. WALTER, F. BACON and F. E. LUBORSKY, *Mater. Sci. Engng* **24** (1976) 239.
8. N. JOST, H. G. HILLENBRAND and E. HORNBOGEN, Proceedings 5th International Conference on Rapidly Quenched Metals, Vol. II (edited by H. Warlimont and S. Steeb) (North Holland, 1985) p. 1417.
9. H. G. HILLENBRAND, E. HORNBOGEN and U. KÖSTER, Proceedings 4th International Conference on Rapidly Quenched Metals, Vol. II (edited by T. Masumoto and K. Suzuki) (Japan Institute of Metals, 1982) p. 1369.
10. A. INOUE, H. TOMIOKA and T. MASUMOTO, *J. Mater. Sci.* **18** (1983) 153.
11. N. MERK, D. G. MORRIS and P. STADELMANN, *Acta Metall.*, in press.
12. M. NAKA, Y. NISHI and T. MASUMOTO, Proceedings 3rd International Conference on Rapidly Quenched Metals, Vol. I, (edited by B. Cantor) (The Metals Society, London, 1978) p. 231.
13. J. REEV, G. P. GREGAN and H. A. DAVIES, Proceedings 5th International Conference on Rapidly Quenched Metals, Vol. I (edited by H. Warlimont and S. Steeb) (1985) p. 203.
14. P. G. ZIELINSKI, J. OSTATEK, M. KIZEK and H. MATYJA, Proceedings 5th International Conference on Rapidly Quenched Metals, Vol. I (edited by B. Cantor) (The Metals Society, London, 1978) p. 337.
15. H. WARLIMONT and P. GORDELIK, Proceedings 5th International Conference on Rapidly Quenched Metals, Vol. I (edited by H. Warlimont and S. Steeb) (North-Holland, 1985) p. 619.
16. P. GORDELIK and F. SOMMER, Proceedings 5th International Conference on Rapidly Quenched Metals, Vol. I. (edited by H. Warlimont and S. Steeb) (North Holland, 1985) p. 623.
17. R. L. FREED and J. B. VAN DER SANDE, *Acta Metall.* **28** (1980), 103.
18. E. SMITH, *ibid.* **14** (1966) 991.
19. T. MASUMOTO and R. MADDIN, *Acta Metall.* **19** (1971) 725.
20. G. R. IRWIN, *Appl. Mater. Res.* **3** (1964) 65.
21. L. A. DAVIS, "Metallic Glasses", (ASM, Metals Park, Ohio, 1978), p. 191.

Received 22 October 1987
and accepted 17 February 1988